
Article:
Smith, R.M. orcid.org/0000-0002-3841-604X and Bigg, G.R. orcid.org/0000-0002-1910-0349 (2023) Impact of giant iceberg A68A on the physical conditions of the surface South Atlantic, derived using remote sensing. Geophysical Research Letters, 50 (18). e2023GL104028. ISSN 0094-8276

https://doi.org/10.1029/2023gl104028

AGU ADVANCING EARTH AND SPACE SCIENCES

Geophysical Research Letters®

RESEARCH LETTER
10.1029/2023GL104028

Impact of Giant Iceberg A68A on the Physical Conditions of the Surface South Atlantic, Derived Using Remote Sensing

R. M. Smith[1,2] and **G. R. Bigg**[3]

[1]British Antarctic Survey, Cambridge, UK, [2]Department of Chemistry, University of Cambridge, Cambridge, UK, [3]Department of Geography, University of Sheffield, Sheffield, UK

Key Points:

- Meltwater released from giant iceberg A68A caused large scale freshening and cooling of the surrounding surface ocean
- Intense temperature and salinity anomalies up to −4.5°C and exceeding −10 psu were recorded during the breakup near South Georgia
- The freshening and cooling signals stretched at times over 1,000 km and persisted for over 2 months following the iceberg's melt

Supporting Information:

Supporting Information may be found in the online version of this article.

Correspondence to:

R. M. Smith,
rosmit19@bas.ac.uk

Citation:

Smith, R. M., & Bigg, G. R. (2023). Impact of giant iceberg A68A on the physical conditions of the surface South Atlantic, derived using remote sensing. *Geophysical Research Letters*, *50*, e2023GL104028. https://doi.org/10.1029/2023GL104028

Received 12 APR 2023
Accepted 17 AUG 2023

Author Contributions:

Conceptualization: G. R. Bigg
Investigation: R. M. Smith
Supervision: G. R. Bigg
Writing – original draft: R. M. Smith
Writing – review & editing: R. M. Smith, G. R. Bigg

Abstract Giant icebergs release cold, fresh meltwater as they drift, perturbing the physical conditions of the surface ocean. This study uses satellite-derived sea surface salinity and temperature measurements to explore the physical impact of supergiant iceberg A68A between September 2020 and June 2021. During A68A's drift through the Scotia Sea in austral spring, gradual but persistent edge-wasting contributed to a freshening of several psu extending hundreds of kilometers ahead of the iceberg, whilst the cooling signal was more pronounced in the iceberg's wake. The magnitude of the physical perturbation intensified during A68A's breakup near South Georgia. Several large meltwater lenses surrounding the descendant icebergs displayed temperature anomalies of up to −4.5°C, whilst the salinity measurements indicated a surface (skin-depth) anomaly regularly exceeding order −10 psu. The perturbations stretched at times >1,000 km and persisted for >2 months following A68A's melt in April 2021.

Plain Language Summary Giant icebergs release cold, fresh meltwater as they drift, altering the conditions of the ocean. This study uses sea surface salinity and temperature data collected by satellites to explore these impacts for iceberg A68 between September 2020 and June 2021. During A68A's drift through the Scotia Sea, a freshening of several psu extended hundreds of kilometers ahead of the iceberg, and a pronounced cooling followed behind. The magnitude of the salinity and temperature anomalies intensified when A68A fragmented near South Georgia. The surface ocean displayed temperature anomalies of up to −4.5°C, and salinity anomalies regularly exceeding −10 psu. The perturbation stretched at times >1,000 km and persisted for >2 months following A68A's melt in April 2021.

1. Introduction

Almost half of the mass loss from the Antarctic ice sheet is in the form of calved icebergs (Depoorter et al., 2013). They release large quantities of cold, fresh water during their drift and decay, perturbing the temperature and salinity conditions of the Southern Ocean. Such perturbations influence sea ice growth (Merino et al., 2016), deep water formation (Robinson & Williams, 2012) and local current patterns (Grosfeld et al., 2001). Iceberg meltwater also delivers nutrients and bioavailable iron to the Southern Ocean, stimulating primary production (Smith et al., 2007).

Over 50% of the iceberg freshwater flux comes from "giant" icebergs exceeding 18 km in length (Tournadre et al., 2016). Although giant icebergs calve episodically, they can survive for years-decades, many persisting until they reach lower latitude waters (Silva et al., 2006). Thus, giant icebergs can impact the Southern Ocean over large spatial and temporal scales.

Several field studies have sought to quantify surface freshening and cooling from individual giant icebergs. Stephenson et al. (2011) observed melting giant (35 × 17 km) iceberg C18A over several weeks in the Weddell Sea. They showed that meltwater is transported both horizontally away from the iceberg, and vertically due to turbulent entrainment of meltwater at the iceberg base. During the same cruise, Helly et al. (2011) measured freshening and cooling signals of 0.5 psu and 0.5°C stretching 19 km away from C18A and persisting for 10 days. Wagner et al. (2018) reported a surface (upper 25 m) depression of ∼1 psu and 3°C within 10 km of a small iceberg field south of New Zealand. In Baffin Bay, Stern et al. (2015) detected an anomalously fresh surface layer (26 psu absolute between 0 and 10 m depth) on one side of grounded iceberg PII-B.

Satellite data are better able to measure an iceberg's long-term evolution. Space-borne instruments are commonly used to observe the physical decay of giant icebergs, as volume lost from the iceberg base and sidewalls over time

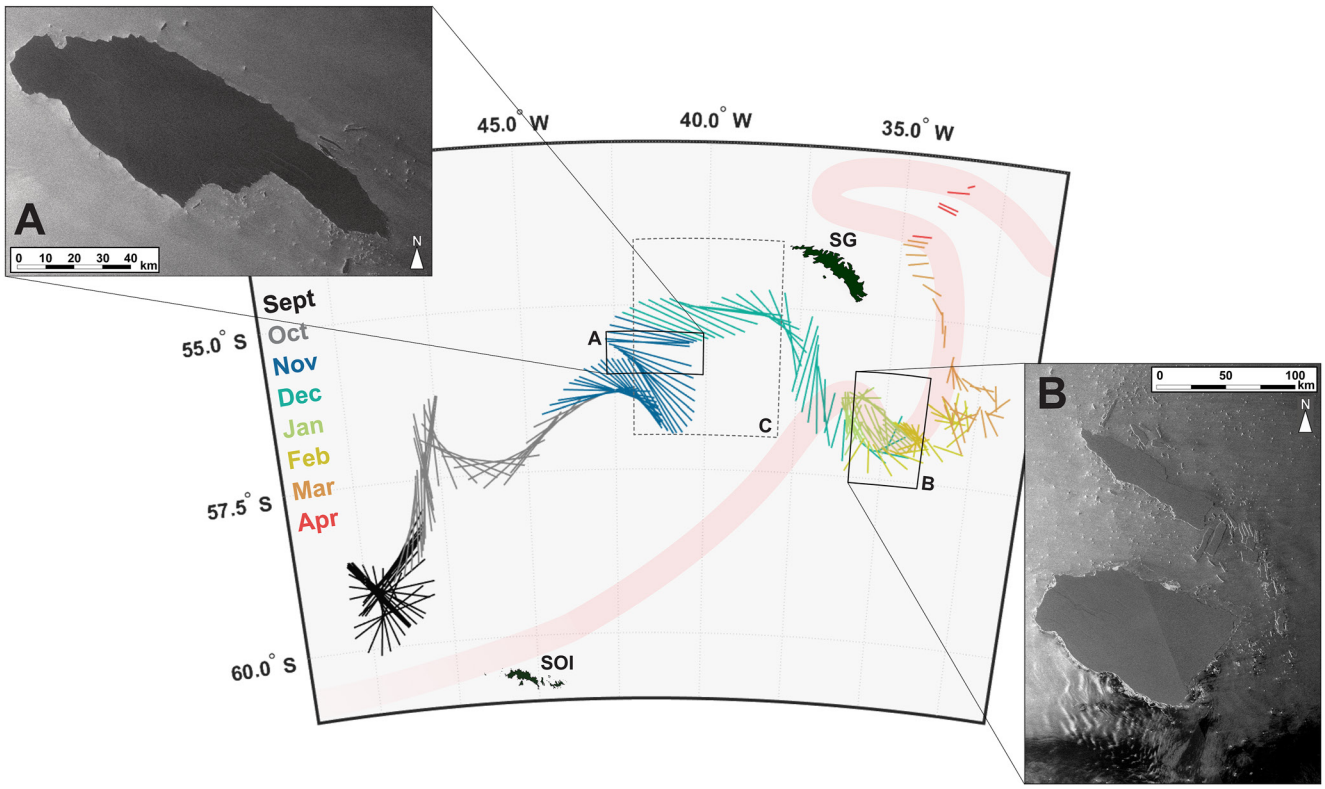

Figure 1. Map showing A68A's trajectory between September 2020 and April 2021. Solid lines denote the orientation of A68A's long axis during the color-coded months. Inset A and B are SAR images acquired by Sentinel 1A on 25 November and 28 December, respectively. Box C denotes where coordinates were selected for the timeseries analysis, Figure 2. Pink band shows the approximate position of the Southern Antarctic Circumpolar Current Front, following from Thorpe et al. (2002). SG = South Georgia, SOI = South Orkney Islands.

(Braakmann-Folgmann et al., 2021; Jansen et al., 2007; Li et al., 2018). Others have examined the impact of the meltwater on the surface ocean. Ocean color data have been used to reveal the regional-scale fertilizing effect of iron-rich iceberg meltwater (Schwarz & Schodlok, 2009; Wu & Hou, 2017), wherein chlorophyll-enriched plumes extending up to 200 km from the iceberg were shown to persist for >1 month (Duprat et al., 2016). Only one study to-date has utilized satellite data to determine the surface freshening and cooling resulting from iceberg meltwater release. Bigg and Marsh (2023) employed sea surface salinity (SSS) measurements (derived from L-band radiometry) to reveal a localized surface freshening of up to 2 psu during the melt of three large (10–20 km-long) icebergs in the South Atlantic. Here, we further test the value of satellite observations for capturing the physical impacts of iceberg meltwater. We focus on a single extremely large iceberg, A68.

In July 2017, A68 calved from the Larsen C Ice Shelf. At 5,800 km^2, it was the sixth largest recorded iceberg (Budge & Long, 2018). A68's drift trajectory was characteristic of Weddell Sea icebergs (Rackow et al., 2017): it was carried north until early 2020, when it reached the edge of the perennial sea ice and was expelled into the Scotia Sea. After calving some relatively small fragments, the largest remaining piece, A68A, then drifted north-eastwards and approached South Georgia in December 2020 (Figure 1). At ~60 km from the coast (on 15 December), it changed course toward the southeast and began a dramatic breakup sequence south of the island. The 13 descendant icebergs (A68D-P) were transported varying distances and directions by the local Southern Antarctic Circumpolar Current Front before melting, between December 2020 and March 2021. The parent iceberg disintegrated on 16 April 2021, 230 km northeast of South Georgia.

Through an assessment of the iceberg's dwindling area and thickness, Braakmann-Folgmann et al. (2022) estimated that 152 ± 61 Gt of meltwater was released between the end of November and early March (when their observations end), within a region up to 300 km from South Georgia. A profound perturbation to the physical conditions of the surrounding ocean is therefore expected, with potential major consequences for surface ocean structure and primary production in the ecologically significant South Georgia region.

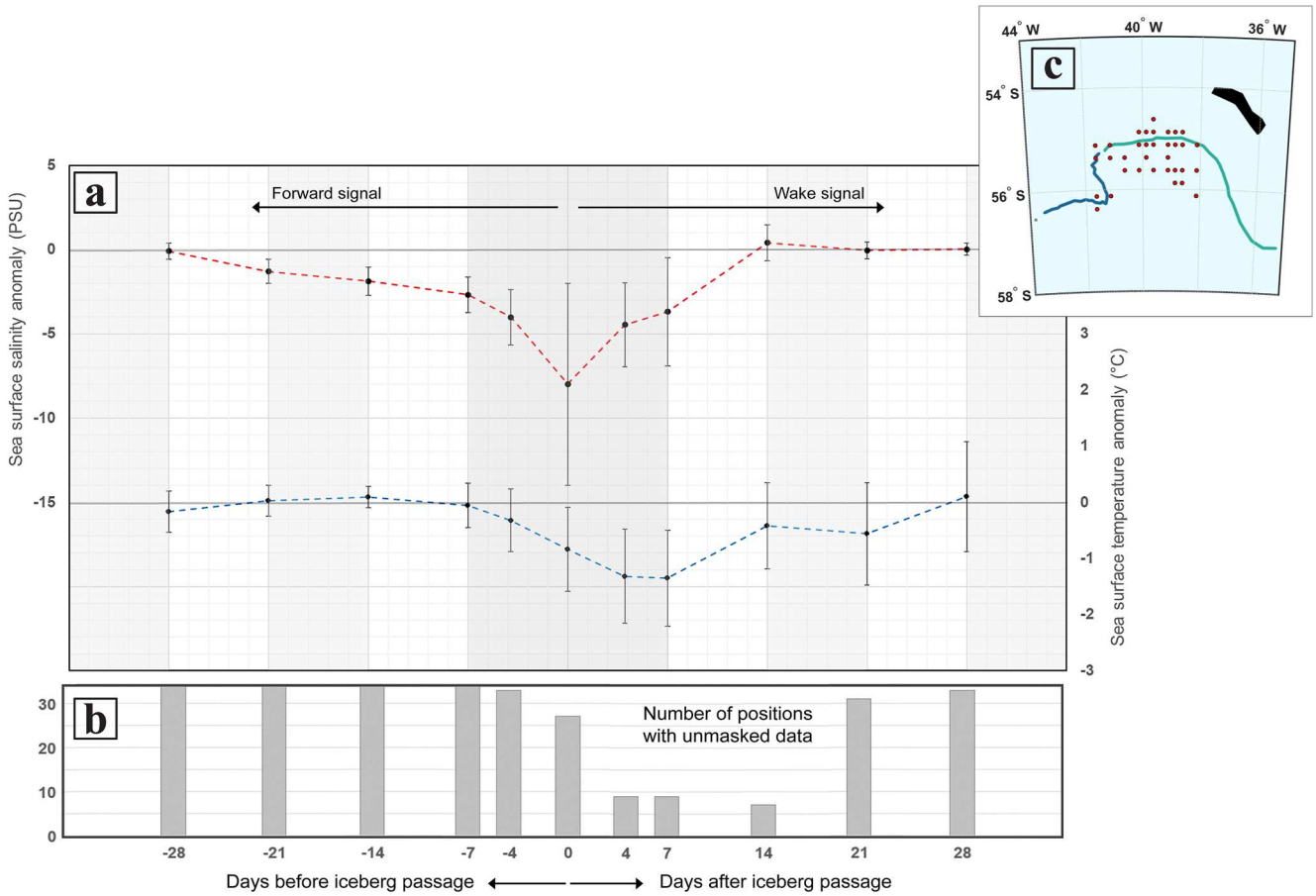

Figure 2. Time series showing the asymmetrical freshening and cooling signals of A68A during austral spring. (a) Average sea surface salinity (SSS) and Sea Surface Temperature anomalies for 34 positions along A68A's spring track, relative to the temporal proximity of the iceberg. Error bars denote standard deviation about the mean. (b) Frequency of unmasked (i.e., available) SSS grid cells, out of 34. Positions were selected between 42–38°W, 54–57°S (see Figure 1, Table S1 in Supporting Information S1).

2. Data and Methods

We focus on the final life stage of A68A, beginning in austral spring (September) 2020 and including the iceberg's final disintegration in autumn (April) 2021. We continued our observations of A68A's residual impact into austral winter (June) 2021; beyond this, diminishing light availability precluded accurate satellite observations.

2.1. Iceberg Tracking

A68 was so large that optical imagery collected by MODIS Aqua and Terra, viewed through NASA Worldview, was sufficient to track the iceberg's daily position. Where necessitated by cloud cover, positions were interpolated based on preceding and subsequent days, assuming constant speed.

2.2. Surface Freshening

The freshening impact of A68 was assessed using SSS retrievals by NASA's Soil Moisture Active Passive (SMAP) satellite, processed and produced by the Jet Propulsion Laboratory (JPL) using their Combined Active/Passive (CAP) algorithm (Fore et al., 2016). JPL's Version 5.0, Level 3, 8-day running mean data were used, with a spatial resolution of 0.25° × 0.25°. Each 8-day product is an average of the preceding and subsequent 96 hr periods, centered at midday on the named day. Monthly climatologies were compiled using data from the SMAP monthly SSS (Level 3 CAP) archive, which commences from April 2015. The resulting climatologies span 2015–2019 for months September–December and April–May. For January–March, climatologies are based on years 2016–2020.

Signal contamination by sea ice is an inevitable challenge in the polar oceans (Fournier et al., 2019). For the JPL SMAP product, sea ice concentration (SIC) ancillary data are acquired in the form of a high resolution (1/12°) daily product from the National Oceanic and Atmospheric Administration (NOAA) National Centers for Environmental Prediction (NCEP), re-gridded to 0.5° × 0.5°. Wherever the SIC value closest to each SMAP footprint exceeds 3% (and additionally within 35 km of land, and where wind speeds exceed 20 m s^{-1}) the SSS value is flagged and filtered (Fore et al., 2020; Tang et al., 2018). Thus, the data presented in this study are frequently masked, including pixels that cover and surround the A68 icebergs. Each Level 3 data set provided by JPL also contains "ice concentration" (where 0%–3%) and SSS "predicted uncertainty" variables. As the ice concentration values are increased surrounding the A68 icebergs throughout the study period, we assume this represents iceberg fragments released by sidewall erosion (rather than in situ sea ice formation) (see note and Figures S1 and S3 in Supporting Information S1). The predicted uncertainty variable is quantified based on propagation of variance within the Level 2 data and includes the effect of cold water and measurement error (amongst other contributors) (Fore et al., 2020). The 50–60°S zonally-averaged estimated error is reported as ∼2.5 psu (Fore et al., 2020), due primarily to the reduced sensitivity of radiometers to salinity in cold waters (Garcia-Eidell et al., 2017). Whilst this degree of uncertainty is substantial, we observe SSS anomalies that exceed their associated estimated error, and argue that whilst the exact SMAP SSS values are to be interpreted with caution, they remain indicative of the overall magnitude and spatial distribution of the A68 freshening signal.

2.3. Surface Cooling

Surface cooling was assessed using the Group for High Resolution Sea Surface Temperature (SST) L4 Global Blended Optimal Interpolation SST Analysis (GDS2), version 2.1. Eight-day averages were created using daily (0.25° × 0.25°) data, matching the temporal and spatial average resolution used by the SMAP 8-day SSS product. Monthly climatologies spanning 2003–2019 were compiled using daily NOAA High-resolution Blended SST Analysis data.

2.4. Surface Currents

The role of currents in controlling iceberg trajectory and meltwater distribution was assessed using the Ocean Surface Current Analysis Real-time product provided by Earth Space Research. Data are available every 5 days. OSCAR's spatial resolution is 1/3° × 1/3°.

3. Results

The impact of A68A proceeded in three distinct phases during the study period: the growth of the meltwater signal throughout austral spring, the summertime signal peak during the breakup sequence, and the autumn-winter signal diminution as the remaining fragments melted. The results are presented according to these stages.

3.1. Austral Spring

From September to December 2020, A68A drifted northeast across the Scotia Sea toward South Georgia (Figure 1). The freshening signal became detectable in November, when a decrease of ∼2 ± 1 psu was recorded ahead of the iceberg (Figure S1 in Supporting Information S1). This meltwater signal was carried by the prevailing currents, forming a "forward" surface plume extending to South Georgia. In the same month, a temperature anomaly of up to −1.5°C was detected close to A68A (Figure S1 in Supporting Information S1). Figure 2 shows SSS and SST anomaly timeseries data for 34 positions along A68A's springtime route, normalized to "day 0," when the iceberg reached (or was closest to) each location. The salinity anomaly was detectable up to 1 month in advance of the iceberg's arrival and dissipated 2 weeks after its passage; the temperature signal showed almost the opposite pattern (Figure 2).

3.2. Austral Summer

By early December, as A68A approached South Georgia, the SSS retrievals showed a substantial anomaly of up to, and exceeding, −9.5 ± 2.1 psu mid-way between the iceberg and island (Figure 3a, red marker). The magnitude of the freshening signal intensified further when moving from the 9 December 8-day average to 10 December; the same position on 10 December showed an increased anomaly of −13.9 ± 3.3 psu, indicative of a super-fresh surface lens stretching 65 km from W-E (Figure 3b). However, note the increased estimated

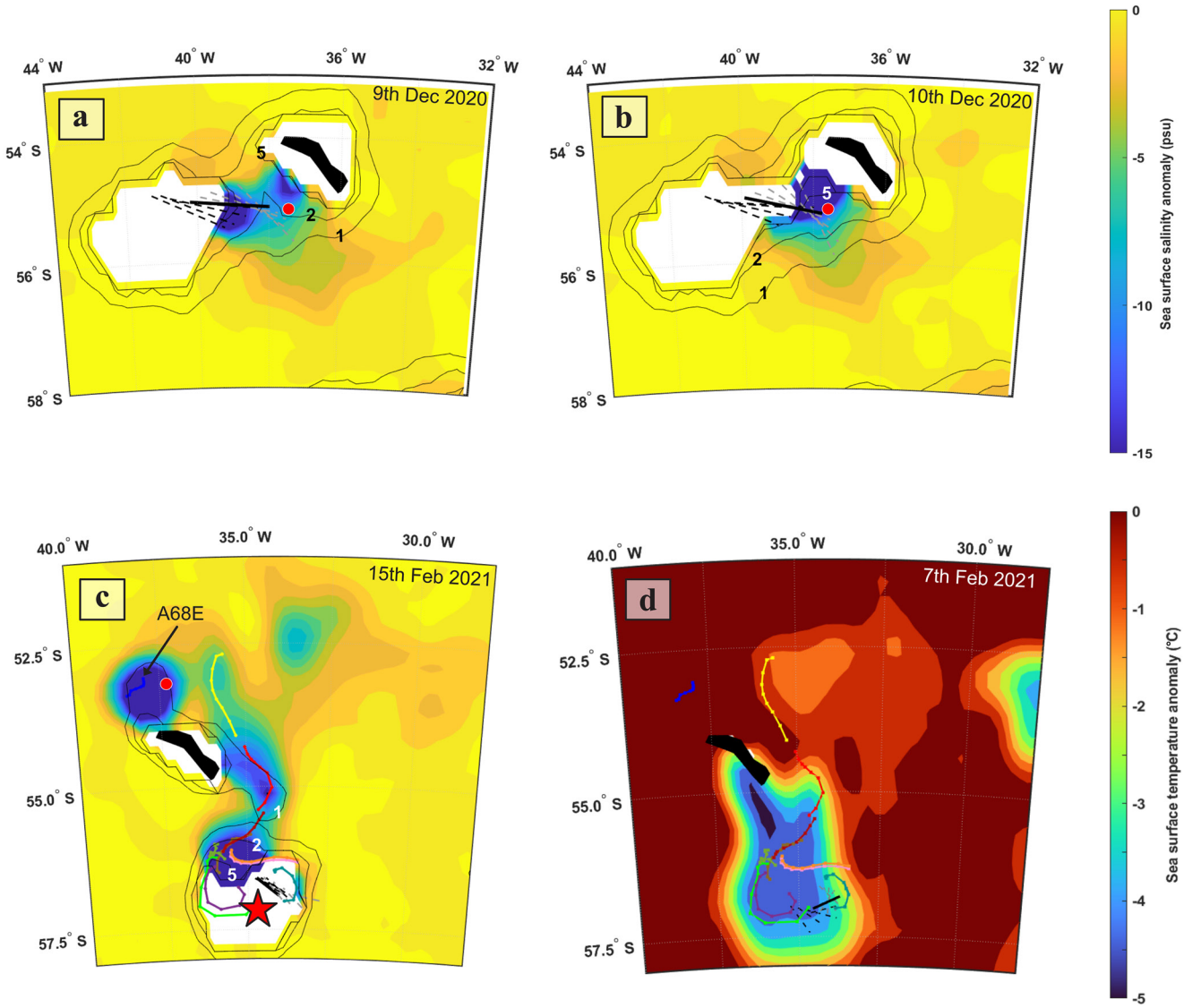

Figure 3. 8-day average anomaly maps. Panels (a)–(c) show sea surface salinity anomalies: white patches are where Soil Moisture Active Passive (SMAP) data is masked by the iceberg/island, elevated sea ice concentration, or cold SSTs; black contours show SMAP estimated uncertainty, spaced at 1, 2, 5, 10 psu (see number labels); red markers show where values reported in text; red star in panel (c) shows center of anticyclonic current. Panel (d) shows Sea Surface Temperature anomaly. Straight black line denotes A68A position on central date, dashed black (gray) lines show preceding (subsequent) 4 days. Colored lines show other iceberg positions during 8-day period (see Figure S2 in Supporting Information S1). Black shape is South Georgia.

error, which coincides with a small jump in SIC. A68A rotated and changed course toward the southeast on 15 December, and A68D calved during this realignment, on 16 December. Throughout the following months, intense salinity anomalies of over −10 psu were common.

In late December, A68A became constrained within a large (>100 km diameter) anticyclonic current centered at 57°S, 35°W (Figure 1b). During A68A's repetitive orbit inside this eddy, the main breakup sequence commenced (Figure S2 in Supporting Information S1). The meltwater distribution became increasingly complex between December-February, when some of the descendant fragments escaped the rotating flow and moved north of South Georgia (Figure 3c; Figure S3 in Supporting Information S1). Distinct freshened lenses with anomalies up to (and occasionally exceeding) −10 psu surrounded each large iceberg (e.g., −19.4 ± 1.2 psu at Figure 3c red marker). In contrast, the SST signal appeared more spatially consistent: a strong anomaly of up to −4.5°C remained focused around the eddy, with a more dispersed cooling to the north (Figure 3d).

3.3. Austral Autumn

In March, the remaining descendant icebergs disintegrated and their residual freshening signal attenuated. A68A itself finally escaped the anticyclonic current in mid-March and moved north of South Georgia in April (Figure 1). A super-fresh surface anomaly (-13.8 ± 1.4 psu at red marker) was detected around A68A as it decayed. The prevailing currents redistributed the freshened water to form a long plume, which lengthened as the injection of meltwater at its western tip continued. In early April the plume extended for 600 km, by the end of April it stretched >1,000 km (Figure 4).

In May, A68A's salinity signal began to diminish. An anomaly of -12.0 ± 1.1 psu was measured on 2nd May, by the 12th this was reduced to -6.3 ± 0.7 psu and by the 28th to -3.6 ± 0.6 psu. This residual −3 psu anomaly persisted throughout June. As austral winter progressed into July, the SSS signal became degraded by the seasonal reduction in SST. Thus, it was not possible to ascertain the date by which A68A's freshening signal fully disappeared.

4. Discussion and Conclusions

The calving of 5,800 km^2 iceberg A68 presents a unique opportunity to assess the oceanic impact of a rare, supergiant iceberg. A68's disintegration caused a substantial perturbation to the physical conditions of the surface ocean near South Georgia, with major potential consequences for surface ocean structure, nutrient supply and productivity in this ecologically significant region.

4.1. Austral Spring: Relationship Between the A68A Cooling and Freshening Signal

The magnitude of A68's SST and SSS signal developed throughout November-December 2020, when the iceberg was drifting through the Scotia Sea. The freshening signal stretched ahead of A68A; the cooling signal was more pronounced in the iceberg's wake (Figure 2). To understand this trend, we consider the mechanisms of freshwater release and redistribution.

Icebergs entering the Scotia Sea experience accelerated basal melting as warmer SSTs drive increased turbulent exchange of heat at the iceberg base (Jansen et al., 2007; Scambos et al., 2008). Accordingly, Braakmann-Folgmann et al. (2022) calculated a rate of volume loss from A68A due to melting of -298.7 ± 94.5 km^3 yr^{-1} in the northern Scotia Sea (compared to -174.2 ± 46.0 km^3 yr^{-1} in the southern Scotia Sea), based on the decreasing thickness of the iceberg. As the heat supplied by the ambient seawater converts the basal ice to meltwater, the seawater is cooled (driving a density increase) and diluted with freshwater (driving a density decrease). The freshening effect dominates and the cold, buoyant meltwater mixture rises through the water column at the iceberg sidewalls, undergoing further mixing, dilution and horizontal redistribution along its upwards trajectory (Stephenson et al., 2011). As suggested by Jansen et al. (2007) for giant iceberg A38B, and originally observed by Foldvik et al. (1980) for smaller bergs, this leads to a persistent plume of freshened water surrounding a freely-drifting berg.

At the iceberg's leading edge, the increased velocity of the surface currents relative to the iceberg's drift act to lengthen this “forward” plume, whilst the rapid melt of the numerous small ice fragments conveyed by this current (and assisted by surface winds; Wagner et al., 2017) contribute additional freshening The plume temperature would initially be cooler than the water displaced beneath, but enhanced stratification favors equilibration with the atmosphere, curtailing the forward plume's temperature signal. The salinity signal, meanwhile, would be better-preserved under these stratified conditions.

In A68A's wake, the mechanical disturbance caused by the movement of a 200 m-deep keel through the water column would cause increased mixing and dilution of the basal meltwater (Helly et al., 2011). The reduced buoyancy of this meltwater mixture favors a more even meltwater distribution throughout the thickened mixed layer, diminishing the magnitude of the surface salinity signal. Conversely, the temperature signal persisted for longer in this “wake” plume; convective overturning and wind-driven mixing throughout the cooled, mixed layer enabled constant replenishment of cold water to the ocean surface.

4.2. Austral Summer: Magnitude of the Freshening Signal

During the austral summer, A68A began to disintegrate; we observed an intensification in the apparent magnitude of the freshening signal, with an extensive salinity anomaly regularly exceeding −10 psu (<24 psu absolute).

10.1029/2023GL104028

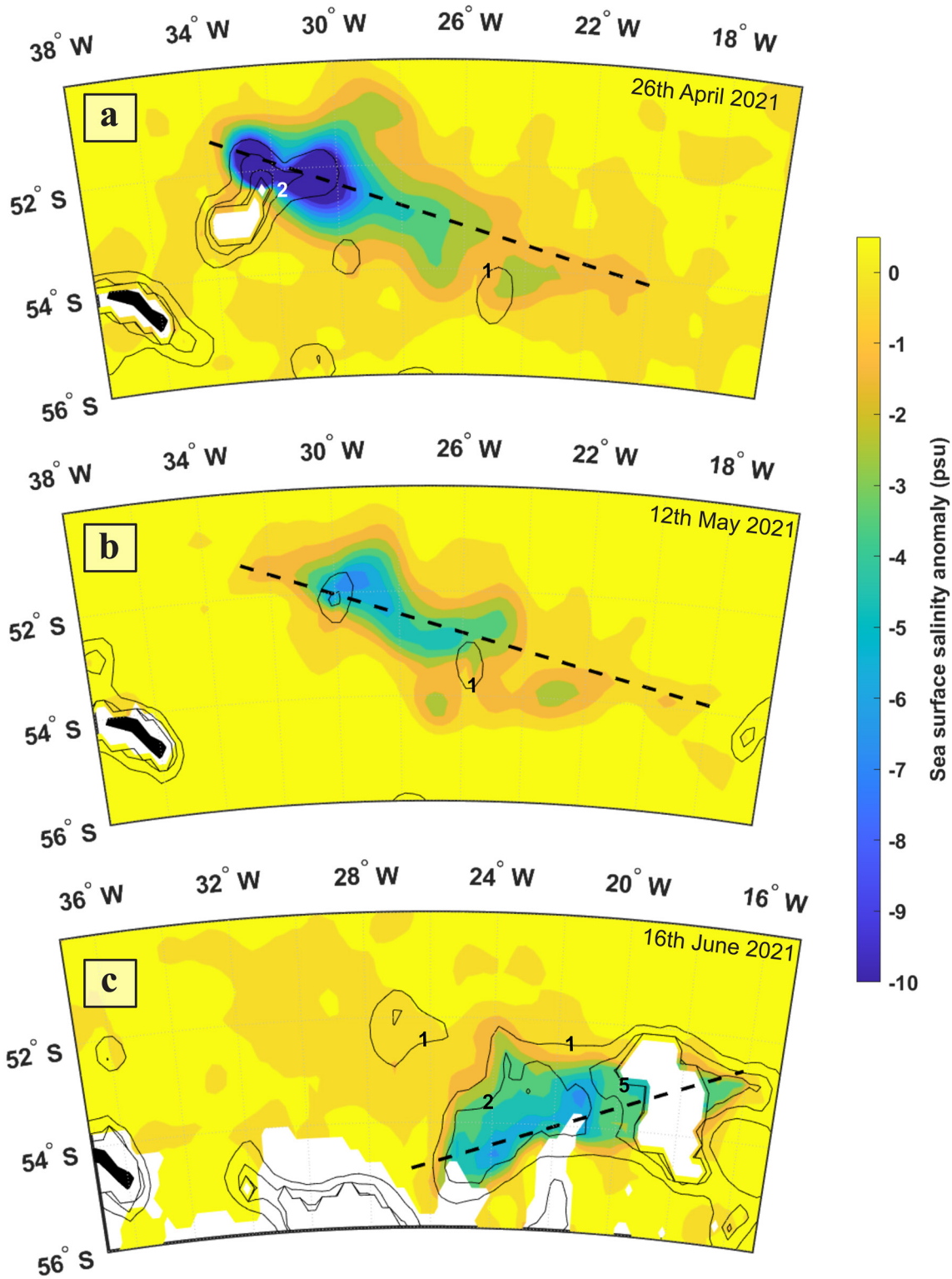

Figure 4. 8-day average sea surface salinity anomaly maps. Black contours are as for Figure 3. Black dashed lines give a sense of scale; in panels (a)–(c) they represent 992, 1,051, and 736 km, respectively. White patches in panel (c) show where the seasonally-reduced SSTs triggered data masking.

This anomaly exceeds the ∼2 psu freshening observed using similar methods by Bigg and Marsh (2023), but their icebergs were an order of magnitude smaller. Turning to the limited number of in situ studies of free-drifting icebergs, a salinity anomaly of −10 psu is without precedent, although most of these studies focus on smaller bergs or colder ambient waters. Given the known limitations of L-band radiometry in cold, ice-rich waters, and assuming additional error introduced by the detection of fine iceberg fragments (as sea ice) throughout the evolving A68 iceberg field, the extreme-low SSS values reported are unlikely to be fully representative of reality, even where the SMAP "estimated uncertainty" remains relatively low.

Fortunately, in situ oceanographic measurements were collected by ship-borne sensors and gliders close to the A68 fragments near South Georgia in early 2021 (Lucas et al., 2022; Meredith et al., 2023). The lowest surface salinity detected by a deployed glider was 25.59 psu, on 4 March 2021, at 56.254°S, 33.243°W, immediately beside A68A (Lucas et al., 2022). Our closest corresponding 8-day mean SSS value is 20.4 ± 7.3 psu (−13.6 psu anomaly), for the grid cell centered at 56.125°S, 33.125°W; the glider measurement falls within the margin of error for our SMAP value, despite the substantial differences in instrumental resolution and measurement depth. However, comparing these two data sources is challenging. Strong vertical gradients in surface salinity are expected near melting icebergs, but whilst "surface" in situ measurements are made at several meters depth, each satellite retrieval relates to the uppermost 1–2cm (sub-skin) (Supply et al., 2020). Rapidly evolving lateral SSS gradients add further complexity; each SMAP "pixel" represents an average over 0.25° × 0.25° (approximately 28 × 16 km at the latitude of interest) and an 8-day period, whilst in situ data are necessarily point-wise in time and space. Neither can fully resolve km-scale horizontal salinity variations in such a dynamic setting.

Regarding the magnitude of the A68 SSS anomaly, a useful comparison can be made with the observed freshening from Arctic river runoff. For example, SMAP is able to resolve the overall magnitude (anomalies up to −15 psu), timing and spatial distribution of surface freshening at the outflow of major Arctic estuaries, despite cold SSTs, potential sea-ice contamination, and satellite versus in situ root mean square differences of 2.85 psu (Tang et al., 2018). We argue that whilst super-fresh SMAP values should be interpreted with caution, the A68-associated SSS perturbation likely exceeded the error introduced by the low SSTs and presence of surface ice, thus a freshening magnitude close to that observed from the Arctic rivers is possible at the sub-skin depth.

4.3. Impact With the South Georgia Shelf

On 14-15 December, at 60 km from South Georgia and with an average draft of 141 ± 11 m (Braakmann-Folgmann et al., 2022), A68A likely impacted with the seafloor when its northern edge passed over a ∼150 m deep bathymetric high. On 16 December, A68D calved from the northern tip of the berg. This sequence also coincided with the earliest detection of the super-fresh anomaly of over −10 psu; a sudden intensification of the freshening signal at the transition between the 9 and 10 December 8-day averages suggests that conditions at the ocean surface changed between midday on 13 and 14 December. The timing of these events leads us to consider whether there was some sudden injection of ice fragments, freshwater, or a mixture of both, to the ocean surface.

Braakmann-Folgmann et al. (2022) used satellite altimeter data to reveal the presence of wide, elongated basal channels orientated along the iceberg's minor axis. It is possible that basal meltwater confined by this uneven iceberg "foot" (whether by these channels, or finer-scale basal crevasses) was rapidly released during the collision. Such an impact would impose additional stress upon the ice body, widening existing fractures and opening new conduits for basal meltwater to escape. Alternatively, the collision may have triggered a sudden release of fine fragments from A68A's sidewalls, contaminating the SMAP-signal, but also accelerating the rate of surface freshening as small pieces melt rapidly at the ocean surface. For both scenarios, the subsequent calving of A68D supports a link between the propagation of the full-thickness rift at the rear of the iceberg, and the sudden intensification of the surface freshening signal.

4.4. Austral Autumn/Winter: Scale of A68A Physical Impact

As A68A disintegrated and the meltwater was redistributed by the prevailing eastward currents, the spatial scale of the salinity anomaly reached a level that is unprecedented in the published literature, with a low-salinity plume stretching >1,000 km across the South Atlantic (Figure 4b). The temporal scale of the physical perturbation is also notable; 2 months after A68A's demise, a surface freshening signal was still detectable within this plume (Figure 4c). As with previous remote sensing studies that exposed the scale of the productivity enhancement from

giant icebergs (Duprat et al., 2016), this finding underlines the value of satellite data in capturing the full spatial and temporal scale of the physical impact of giant icebergs.

5. Conclusion

This study utilized satellite data to capture the freshening and cooling impact of supergiant iceberg A68A. This method has proven particularly valuable for capturing large-scale lateral gradients in surface salinity and temperature, that intensified in austral summer during A68A's breakup, and that persisted for >2 months after the iceberg's melt. A series of freshened lenses were detected surrounding each melting fragment, with sub-skin anomalies exceeding −10 psu, although error introduced by cold SSTs and iceberg fragments means the true magnitude of these surface anomalies remains uncertain. Efforts are underway to improve the accuracy of L-band SSS in cold, ice-rich polar oceans (Kolodziejczyk et al., 2021; Supply et al., 2020) including enhanced sea ice filtering and SST corrections. We suggest that melting icebergs may provide a useful future testing ground for this work, particularly as a growing number of iceberg field studies - motivated by a need to understand the consequences of increasing ice shelf calving and collapse - may improve the availability of ground-truthing data.

Conflict of Interest

The authors declare no conflicts of interest relevant to this study.

Data Availability Statement

All data used in this study are freely available online. SMAP salinity data are available at https://doi.org/10.5067/SMP50-3TPCS. GHRSST temperature data are available at https://doi.org/10.5067/GHAAO-4BC21. OSCAR current data are available at https://doi.org/10.5067/OSCAR-03D01. Sentinel 1A and 1B SAR data are available via the ESA Copernicus Open Access Hub (https://scihub.copernicus.eu/). Daily positions of icebergs A68A and A68D-P, recorded for this work using NASA MODIS Aqua and Terra optical imagery available at https://worldview.earthdata.nasa.gov, are freely available via the UK Polar Data Centre (https://doi.org/10.5285/d56d9e3f-80d2-4076-9e70-24f662c0e362).

Acknowledgments

We are grateful to N. Lucas for providing their glider measurements and for their constructive advice during the drafting of this paper. Much of this work was carried out during the Sheffield-based MSc(Res) dissertation of R. M. Smith, but the work was completed, prepared and submitted during their NERC-funded PhD at the British Antarctic Survey and University of Cambridge. This paper was supported by NERC core funding to BAS.

References

Bigg, G. R., & Marsh, R. (2023). The history of a cluster of large icebergs on leaving the Weddell Sea pack ice and their impact on the ocean. *Antarctic Science*, *35*(3), 1–18. https://doi.org/10.1017/S0954102022000517

Braakmann-Folgmann, A., Shepherd, A., Gerrish, L., Izzard, J., & Ridout, A. (2022). Observing the disintegration of the A68A iceberg from space. *Remote Sensing of Environment*, *270*(112855), 112855. https://doi.org/10.1016/J.RSE.2021.112855

Braakmann-Folgmann, A., Shepherd, A., & Ridout, A. (2021). Tracking changes in the area, thickness, and volume of the Thwaites tabular iceberg "B30" using satellite altimetry and imagery. *The Cryosphere*, *15*(8), 3861–3876. https://doi.org/10.5194/tc-15-3861-2021

Budge, J. S., & Long, D. G. (2018). A comprehensive database for Antarctic iceberg tracking using scatterometer data. *Ieee Journal of Selected Topics in Applied Earth Observations and Remote Sensing*, *11*(2), 434–442. https://doi.org/10.1109/JSTARS.2017.2784186

Depoorter, M. A., Bamber, J. L., Griggs, J. A., Lenaerts, J. T. M., Ligtenberg, S. R. M., van den Broeke, M. R., & Moholdt, G. (2013). Calving fluxes and basal melt rates of Antarctic ice shelves. *Nature*, *502*(7469), 89–92. https://doi.org/10.1038/nature12567

Duprat, L. P. A. M., Bigg, G. R., & Wilton, D. J. (2016). Enhanced Southern Ocean marine productivity due to fertilization by giant icebergs. *Nature Geoscience*, *9*(3), 219–221. https://doi.org/10.1038/ngeo2633

Foldvik, A., Gammelsrød, T., & Gjessing, Y. (1980). Measurements of the radiation temperature of Antarctic icebergs and the surrounding surface water. *Annals of Glaciology*, *1*, 19–22. https://doi.org/10.3189/s026030550001689x

Fore, A. G., Yueh, S. H., Tang, W., & Hayashi, A. K. (2020). *SMAP salinity and wind speed data user's guide: Version 5.0*. Jet Propulsion Laboratory. Retrieved from https://podaac-tools.jpl.nasa.gov/drive/files/allData/smap/docs/%20JPL-CAP_V5/SMAP-SSS_JPL_V5.0_Documentation.pdf

Fore, A. G., Yueh, S. H., Tang, W., Stiles, B. W., & Hayashi, A. K. (2016). Combined active/passive retrievals of ocean vector wind and sea surface salinity with SMAP. *IEEE Transactions on Geoscience and Remote Sensing*, *54*(12), 7396–7404. https://doi.org/10.1109/TGRS.2016.2601486

Fournier, S., Lee, T., Tang, W., Steele, M., & Olmedo, E. (2019). Evaluation and intercomparison of SMOS, Aquarius, and SMAP Sea surface salinity products in the Arctic Ocean. *Remote Sensing*, *11*(24), 3043. https://doi.org/10.3390/rs11243043

Garcia-Eidell, C., Comiso, J. C., Dinnat, E., & Brucker, L. (2017). Satellite observed salinity distributions at high latitudes in the Northern Hemisphere: A comparison of four products. *Journal of Geophysical Research: Oceans*, *122*(9), 7717–7736. https://doi.org/10.1002/2017JC013184

Grosfeld, K., Schröder, M., Fahrbach, E., Gerdes, R., & Mackensen, A. (2001). How iceberg calving and grounding change the circulation and hydrography in the Filchner Ice Shelf-Ocean System. *Journal of Geophysical Research*, *106*(C5), 9039–9055. https://doi.org/10.1029/2000JC000601

Helly, J. J., Kaufmann, R. S., Stephenson, G. R., & Vernet, M. (2011). Cooling, dilution and mixing of ocean water by free-drifting icebergs in the Weddell Sea. *Deep-Sea Research Part II Topical Studies in Oceanography*, *58*(11–12), 1346–1363. https://doi.org/10.1016/j.dsr2.2010.11.010

Jansen, D., Schodlok, M., & Rack, W. (2007). Basal melting of A-38B: A physical model constrained by satellite observations. *Remote Sensing of Environment*, *111*(2), 195–203. https://doi.org/10.1016/j.rse.2007.03.022

Kolodziejczyk, N., Hamon, M., Boutin, J., Vergely, J.-L., Reverdin, G., Supply, A., & Reul, N. (2021). Objective analysis of SMOS and SMAP Sea surface salinity to reduce large-scale and time-dependent biases from low to high latitudes. *Journal of Atmospheric and Oceanic Technology*, *38*(3), 405–421. https://doi.org/10.1175/JTECH-D-20-0093.1

Li, T., Shokr, M., Liu, Y., Cheng, X., Li, T., Wang, F., & Hui, F. (2018). Monitoring the tabular icebergs C28A and C28B calved from the Mertz Ice Tongue using radar remote sensing data. *Remote Sensing of Environment*, *216*, 615–625. https://doi.org/10.1016/j.rse.2018.07.028

Lucas, N., Brearley, A., Abrahamsen, P., Meredith, M., Hendry, K., Manno, C., et al. (2022). Physical, biogeochemical and ecological impacts of giant icebergs: A multidisciplinary study of iceberg A68 near South Georgia, Southern Ocean. *Paper presented at EGU general assembly 2022, Vienna, Austria, 23–27 May 2022, EGU22-3914*. https://doi.org/10.5194/EGUSPHERE-EGU22-3914

Meredith, M. P., Povl Abrahamsen, E., Alexander Haumann, F., Leng, M. J., Arrowsmith, C., Barham, M., et al. (2023). Tracing the impacts of recent rapid sea ice changes and the A68 megaberg on the surface freshwater balance of the Weddell and Scotia Seas. *Philosophical Transactions of the Royal Society A*, *381*(2249), 381. https://doi.org/10.1098/RSTA.2022.0162

Merino, N., le Sommer, J., Durand, G., Jourdain, N. C., Madec, G., Mathiot, P., & Tournadre, J. (2016). Antarctic icebergs melt over the Southern Ocean: Climatology and impact on sea ice. *Ocean Modelling*, *104*, 99–110. https://doi.org/10.1016/j.ocemod.2016.05.001

Rackow, T., Wesche, C., Timmermann, R., Hellmer, H. H., Juricke, S., & Jung, T. (2017). A simulation of small to giant Antarctic iceberg evolution: Differential impact on climatology estimates. *Journal of Geophysical Research: Oceans*, *122*(4), 3170–3190. https://doi.org/10.1002/2016JC012513

Robinson, N. J., & Williams, M. J. M. (2012). Iceberg-induced changes to polynya operation and regional oceanography in the southern Ross Sea, Antarctica, from in situ observations. *Antarctic Science*, *24*(5), 514–526. https://doi.org/10.1017/S0954102012000296

Scambos, T., Ross, R., Bauer, R., Yermolin, Y., Skvarca, P., Long, D., et al. (2008). Calving and ice-shelf break-up processes investigated by proxy: Antarctic tabular iceberg evolution during northward drift. *Journal of Glaciology*, *54*(187), 579–591. https://doi.org/10.3189/002214308786570836

Schwarz, J. N., & Schodlok, M. P. (2009). Impact of drifting icebergs on surface phytoplankton biomass in the Southern Ocean: Ocean colour remote sensing and in situ iceberg tracking. *Deep-Sea Research Part I Oceanographic Research Papers*, *56*(10), 1727–1741. https://doi.org/10.1016/j.dsr.2009.05.003

Silva, T. A. M., Bigg, G. R., & Nicholls, K. W. (2006). Contribution of giant icebergs to the Southern Ocean freshwater flux. *Journal of Geophysical Research*, *111*(C3), C03004. https://doi.org/10.1029/2004JC002843

Smith, K. L., Robison, B. H., Helly, J. J., Kaufmann, R. S., Ruhl, H. A., Shaw, T. J., et al. (2007). Free-drifting icebergs: Hot spots of chemical and biological enrichment in the Weddell Sea. *Science*, *317*(5837), 478–482. https://doi.org/10.1126/science.1142834

Stephenson, G. R., Sprintall, J., Gille, S. T., Vernet, M., Helly, J. J., & Kaufmann, R. S. (2011). Subsurface melting of a free-floating Antarctic iceberg. *Deep-Sea Research Part II Topical Studies in Oceanography*, *58*(11–12), 1336–1345. https://doi.org/10.1016/j.dsr2.2010.11.009

Stern, A. A., Johnson, E., Holland, D. M., Wagner, T. J. W., Wadhams, P., Bates, R., et al. (2015). Wind-driven upwelling around grounded tabular icebergs. *Journal of Geophysical Research: Oceans*, *120*(8), 5820–5835. https://doi.org/10.1002/2015JC010805

Supply, A., Boutin, J., Vergely, J. L., Kolodziejczyk, N., Reverdin, G., Reul, N., & Tarasenko, A. (2020). New insights into SMOS Sea surface salinity retrievals in the Arctic Ocean. *Remote Sensing of Environment*, *249*, 112027. https://doi.org/10.1016/J.RSE.2020.112027

Tang, W., Yueh, S., Yang, D., Fore, A., Hayashi, A., Lee, T., et al. (2018). The potential and challenges of using Soil Moisture Active Passive (SMAP) sea surface salinity to monitor Arctic Ocean freshwater changes. *Remote Sensing*, *10*(6), 869. https://doi.org/10.3390/rs10060869

Thorpe, S. E., Heywood, K. J., Brandon, M. A., & Stevens, D. P. (2002). Variability of the southern Antarctic circumpolar current front north of South Georgia. *Journal of Marine Systems*, *37*(1–3), 87–105. https://doi.org/10.1016/S0924-7963(02)00197-5

Tournadre, J., Bouhier, N., Girard-Ardhuin, F., & Rémy, F. (2016). Antarctic icebergs distributions 1992–2014. *Journal of Geophysical Research: Oceans*, *121*(1), 327–349. https://doi.org/10.1002/2015JC011178

Wagner, T. J. W., Dell, R. W., & Eisenman, I. (2017). An analytical model of iceberg drift. *Journal of Physical Oceanography*, *47*(7), 1605–1616. https://doi.org/10.1175/JPO-D-16-0262.1

Wagner, T. J. W., Dell, R. W., Eisenman, I., Keeling, R. F., Padman, L., & Severinghaus, J. P. (2018). Wave inhibition by sea ice enables trans-Atlantic ice rafting of debris during Heinrich events. *Earth and Planetary Science Letters*, *495*, 157–163. https://doi.org/10.1016/J.EPSL.2018.05.006

Wu, S.-Y., & Hou, S. (2017). Impact of icebergs on net primary productivity in the Southern Ocean. *The Cryosphere*, *11*(2), 707–722. https://doi.org/10.5194/tc-11-707-2017

References From the Supporting Information

Reul, N., Grodsky, S. A., Arias, M., Boutin, J., Catany, R., Chapron, B., et al. (2020). Sea surface salinity estimates from spaceborne L-band radiometers: An overview of the first decade of observation (2010–2019). *Remote Sensing of Environment*, *242*(111769), 111769. https://doi.org/10.1016/j.rse.2020.111769